ORNL/TM-2014/439

Microstructure and Basic Mechanical Properties of the Procured Advanced Alloys for the Advanced Radiation Resistant Materials Program

Lizhen Tan
David T. Hoelzer
Jeremy T. Busby

September 22, 2014

OAK RIDGE NATIONAL LABORATORY
MANAGED BY UT-BATTELLE FOR THE US DEPARTMENT OF ENERGY

ORNL/TM-2014/439

Light Water Reactor Sustainability (LWRS) Program

MICROSTRUCTURE AND BASIC MECHANICAL PROPERTIES OF THE PROCURED ADVANCED ALLOYS FOR THE ADVANCED RADIATION RESISTANT MATERIALS PROGRAM

Lizhen Tan, David T. Hoelzer, Jeremy T. Busby

Date Published: September 22, 2014

Prepared by
OAK RIDGE NATIONAL LABORATORY
Oak Ridge, Tennessee 37831-6283
managed by
UT-BATTELLE, LLC
for the
US DEPARTMENT OF ENERGY
under contract DE-AC05-00OR22725

CONTENTS

Page

LIST OF FIGURES

Figure **Page**

LIST OF TABLES

Table **Page**

ACKNOWLEDGMENTS

This research was sponsored by the U.S. Department of Energy, Office of Nuclear Energy, for the Light Water Reactor Sustainability (LWRS) program Research and Development effort. This research was supported in part by the Office of Nuclear Energy, Science and Technology and by the Center for Nanophase Materials Sciences (CNMS), which is sponsored by the Scientific User Facilities Division, Office of Basic Energy Sciences, U.S. Department of Energy.

The authors are grateful to Larry Nelson of JLN Consulting for organizing and coordinating this program, Martin Morra of GE for helpful discussion and sharing/connecting industrial vendors, Kevin Field of ORNL for reviewing this report, and Eric Manneschmidt, David Harper, Gregory Cox, and Tom Geer of ORNL for preparing the samples.

EXECUTIVE SUMMARY

Life extension of the existing nuclear reactors imposes high fluence irradiation to structural materials, resulting in significant challenges to the traditional reactor materials such as type 304 and 316 stainless steels. Advanced alloys with superior radiation resistance will increase safety margins, design flexibility, and economics for not only the life extension of the existing fleet but also new builds with advanced reactor designs. The Electric Power Research Institute (EPRI) has teamed up with Department of Energy (DOE) to initiate the Advanced Radiation Resistant Materials (ARRM) program, targeting to develop and test a degradation resistant alloy from current commercial alloy specifications by 2021 and to a new advanced alloy with superior degradation resistance in light water reactor (LWR)-relevant environments by 2024.

A total of sixteen downselected commercial and advanced alloys are being procured for testing under the ARRM program. EPRI-GE (General Electric) is leading the procurement of eleven commercial alloys. Most of the commercial alloys (eight out of eleven) have been procured. Oak Ridge National Laboratory (ORNL) is leading the procurement of advanced alloys, including customized Grade 92, customized alloy 439, 14YWT oxide-dispersion-strengthened (ODS) alloy, and two other alloys that are to be determined in the alloy groups of 12Cr ferritic-martensitic (FM) steel and high-Cr&Al ODS alloy. The procured commercial and advanced alloys will be stored and organized at EPRI and ORNL, respectively. A material tracking system is being established and used at EPRI and ORNL during the progress of the ARRM program.

The customized Grade 92 and alloy 439, fabricated by means of vacuum induction melting (VIM), electro-slag remelting (ESR) and hot forging, have been procured from Carpenter Technology Corporation (CarTech). Each alloy has a nominal cast weight of 400 lbs. and is in the form of 5 cm-thick plates. The 14YWT ODS alloy (~4.5 kg) has been extruded, cross-rolled and decanned at ORNL. Additionally, reference alloys, i.e., 316L and T92 (tube form of NF616) have been procured from another two vendors.

The procured heats of Grade 92 and alloy 439 have been assessed according to relevant ASTM standards and general materials quality requirements, e.g., chemistry homogeneity, microstructural uniformity, tensile, hardness, and Charpy impact resistance. The as-received Grade 92 showed good chemistry control for the VIM heat (#011448). The additional ESR process resulted in significant reductions in the amounts of Si, Nb, N, and B of the VIM+ESR heat (#011442). Samples of heat #011448 exhibited tempered martensite uniformly developed in the material. The hardness and yield strength of the heat are greater than the requirements specified in the ASTM A182-12a, leading to a low absorbed Charpy impact energy at room temperature. Experiments on additional tempering of the samples indicated that a total of 4 hr tempering at 750°C will provide balanced properties in terms of Charpy impact resistance and strength. Therefore, this type of additional tempering has been applied to the plates of heat #011448. Similar studies on heat #011442 will be pursued.

The as-received alloy 439 heat (#011438) exhibited chemistry and hardness satisfying ASTM A240-13a. The grain size across plate thickness ranges from ~200 μm at surfaces to about 1-2 mm at plate center. To obtain refined grain size with much smaller size variations, thermomechanical treatment (TMT) has been conducted on small pieces of the alloy 439. It has shown that lower temperature warm rolling, e.g., 500°C, developed recrystallized grains in the order of 100 μm in most of the processed material. Further TMT studies will be conducted to obtain completely recrystallized microstructure in alloy 439.

Six plates (approximately 12 × 7 × 0.9 cm^3 each) of 14YWT ODS alloy, recently renamed as FCRD-NFA1 (Fuel Cycle Research & Development – Nano-structured Ferritic Alloy), have been produced by extruding ball milled powder at 850ºC and cross-rolling to 50% thickness reduction. The plates were produced using the "best practice" processing conditions developed in the FCRD Advanced Fast Reactor Cladding Program and the extrusion and rolling conditions developed over the past 12 years at ORNL from producing numerous heats of the advanced 14YWT ODS ferritic alloy. The conditions consisted of an unique Ar gas atomization approach that introduced Y into the pre-alloyed (Fe - 13.8Cr - 3.0W - 0.37Ti - 0.21Y - 0.012O; wt. %) powder melt and improved ball milling conditions, resulting in lower C and N contamination levels and better control in the O level of the powder. Characterization studies of the microstructure and basic mechanical properties of the FCRD-NFA1 were initiated. The grain structure observed by scanning electron microscopy (SEM) analysis consisted of sub-micron size grains that were equiaxed in the longitudinal-transverse (LT) orientation with a grain aspect ratio (GAR) of ~1 and elongated in the longitudinal-normal (LN) orientation with a GAR of ~1.7, due to the effects of cross-rolling (former) and 50% thickness reduction (latter) on the grain morphology. The hardness measurements were consistent by showing no macroscopic variations in the microstructure. However, the results also showed a higher than normal concentration of ~20-150 nm size particles (believed to of the Ti(O,C,N) distributed in wavy patterns in the microstructure (LT orientation) and a modest bimodal grain size distribution. Both of these results may indicate that the Ti content of future alloy development efforts may need to be lowered.

1. BACKGROUND

Nuclear power currently provides a significant fraction of the United States' non-carbon emitting power generation. In future years, nuclear power must continue to generate a significant portion of the nation's electricity to meet the growing electricity demand, clean energy goals, and ensure energy independence. New reactors will be an essential part of the expansion of nuclear power. However, given limits on new builds imposed by economics and industrial capacity, the extended service of the existing fleet will also be required.

Nuclear reactors present a very harsh environment for components service. Components within a reactor core must tolerate high temperatures, water, stress, vibration, and an intense neutron field. The nominal irradiation temperature in light water reactors (LWRs) is ~290°C; however, actual component temperatures range from 270°C to 370°C depending on the relative position of the component within the reactor core and relative amounts of cooling and gamma heating. Degradation of materials in this environment can lead to reduced performance, and in some cases, sudden failure.

Extending the service life of a reactor will increase the total neutron fluence to each component and may result in irradiation-induced effects not yet observed in LWR conditions, although this form of degradation has been observed in fast reactor conditions. Irradiation-induced processes must be carefully considered for higher fluences, particularly the influence of radiation-induced segregation (RIS), swelling, and/or precipitation on embrittlement. The neutron irradiation field can produce large property and dimensional changes in materials. For LWRs, high temperature embrittlement and creep are not common problems due to the lower reactor temperature. However, radiation embrittlement, phase transformation, segregation, and swelling have all been observed in reactor components.

Under irradiation, the large concentrations of radiation-induced defects will diffuse to defect sinks such as grain boundaries and free surfaces. These concentrations are in far excess of thermal-equilibrium values and can lead to coupled-diffusion with particular atoms. In engineering metals such as stainless steel, this results in RIS of elements within the steel. For example, in type 316 stainless steel, chromium (important for corrosion resistance) can be depleted at areas while elements like nickel and silicon are enriched to levels well above the starting, homogenous composition. While RIS does not directly cause component failure, it can influence corrosion behavior in a water environment.

Irradiation-induced changes of alloy microstructure may also lead to hardening and susceptibility to mechanical failure. Further, this form of degradation can accelerate the thermally-driven phase transformations and also result in phase transformations that are not favorable under thermal aging. Phase transformations have been observed in a variety of materials and operating conditions of austenitic steels in LWRs that may impact component lifetime as plants strive towards longer lifetimes. This form of degradation may become visible in a number of components including core barrels, baffle plates, baffle bolts, top guides, and support plates. All of these components are made from austenitic stainless steels including 304, 316, and 347 grades. Of these grades, 316 may be the most susceptible to the formation of G and γ' phases due to the higher Ni content. 304 and 347 may be more likely to undergo martensitic transformations due to their lower austenite stability. Additional neutron fluence may exacerbate radiation-induced phase transformations and should be considered. Comprehensive reviews on radiation effects on the traditional structural materials of LWRs can be found in Ref. [1,2].

Therefore, advanced alloys are desirable, which have greater radiation resistance than the traditional reactor materials. The use of such advanced alloys in replacing the traditional reactor materials for the extension of the existing fleets and the building of new reactors will bring improved safety margins and economics. To identify and develop advanced radiation resistant materials, Electric Power Research

Institute (EPRI) has teamed up with Department of Energy (DOE) to initiate an Advanced Radiation-Resistant Materials (ARRM) program. The EPRI report of "Critical Issues Report and Roadmap for the Advanced Radiation-Resistant Materials Program" [3] reviewed the current commercial and advanced alloys that are applicable as core structural materials of LWRs and laid out a detailed research plan to meet the goal of the program. A number of alloys were down-selected as candidate materials to be tested in the ARRM program, managed by Drs. R. Pathania of EPRI and J.T. Busby of Oak Ridge National Laboratory (ORNL). Procurement of high quality alloys of the candidate materials is essential to successfully implement the program. The alloy procurement processes have followed the EPRI-ARRM materials procuring guidance, ORNL Quality Assurance process equivalent to ASME NQA-1 standard, and ASTM standards that are relevant to specific alloys and testing methods. The identified alloys that are to be procured are classified into two categories, i.e., commercial alloys and advanced alloys, listed in Table 1. Commercial reference alloys are also listed in Table 1.

Table 1. Identified commercial, advanced, and reference alloys to be procured for testing in the ARRM program.

	Commercial Alloys
Ni-base	C22, 690, 625, 625-plus (age hardened), X-750, 725, 718
Austenitic	800, 309/310
Others	Zr-2.5Nb, Ti alloys (Grade 26 with 0.1 Ru)
	Advanced Alloys
9Cr FM[1]	Grade 92
12Cr FM	To be determined, *e.g., HT-9, HCM12A*
High-Cr (>14Cr) Ferritic	439
9-14Cr ODS[2]	14YWT
High-Cr&Al ODS	To be determined, *e.g., PM2000, MA956, 16-ODS*
	Reference Alloys
Austenitic	304L, 316L
9Cr FM	T92 (NF616)

[1] FM: ferritic-martensitic
[2] ODS: oxide-dispersion-strengthened

EPRI and General Electric (GE) are leading the procurement of the commercial alloys. ORNL is leading the procurement of the advanced alloys and reference alloys. The procured alloys will be examined in terms of chemistry homogeneity, microstructural uniformity, and basic mechanical properties to justify their qualities according to relevant ASTM standards. All the procured commercial and advanced alloys will be stored and organized at EPRI and ORNL, respectively.

The commercial alloys C22, 625, 625-plus, 690, 718, 725, X-750, and Zr-2.5Nb have been or being procured from Carpenter Technology Corporation, ATI Teledyne Wah-Chang, and Knolls Atomic Power Laboratory (KAPL). Vendors who can supply the other commercial alloys, i.e., 800, 309/310, and Ti alloy, are being contacted. The detailed procurement status of the advanced alloys is presented in this report.

2. PROCUREMENT OF ADVANCED ALLOYS

The procurement of Grade 92 (9Cr FM), alloy 439 (high-Cr ferritic), 14YWT (9-14Cr ODS), and other advanced alloys are discussed here.

2.1 Grade 92 (9Cr FM)

Grade 92 was down-selected in the 9Cr FM steel category. It was initially developed by Nippon Steel of Japan with a designation of NF616. According to the forms of the material, Grade 92 is specified in different designations of the ASTM and ASME standards. Table 2 lists the applicable ASTM and ASME standards of Grade 92. Grade 92 is also included in the ASME Boiler & Pressure Vessel Code Section I and VIII Division I. Pressure vessels and pipes are usually fabricated by hot forging. According to the ASTM A182, hot forged plates, designated as F92 (UNS K92460), are required to be heat treated by normalization at 1040-1080°C followed by air cooling and tempering at 730-800°C.

Table 2. ASTM and ASME designations of Grade 92.

Material Form	Standards
Forged or rolled plate/pipe	ASTM A182, ASME SA182, ASME SA369
Pipe	ASTM A335, ASME SA335
Tube	ASTM A213, ASME SA213
Pressure Vessel	ASTM A1017

Customized Grade 92 has being developed under the DOE-NE Advanced Reactor Concept (ARC) program for the Sodium-Cooled Fast Reactor. The customized Grade 92 has shown noticeably improved tensile and creep performance with similar performance on fatigue, creep-fatigue, fracture toughness, and weldability as compared to conventional P/T92. The customized Grade 92 is selected in the alloy group of 9Cr FM steels for testing in the ARRM program due to the improved properties over conventional P/T92. Scale up heats of the customized Grade 92 has been procured from the R&D Department of Carpenter Technology Corporation (CarTech) under the ARC program. The same vendor has been used in heats procurement under the ARRM program.

Two heats (#011442 and #011448) of customized Grade 92 in a form of forged plates have been procured from CarTech. Figure 1 shows the two plates of heat #011442. The processing of the heats is summarized in Table 3. Vacuum induction melting (VIM) and electro-slag remelting (ESR) were employed in producing heat #011442, but only VIM was used for heat #011448. The VIM yielded an 20.3 cm-diameter ingot while the ESR yielded a 19 cm × 19 cm square billet. The normalization temperature is higher than that specified in the ASTM A182 to allow complete dissolution of precipitates into solid solution of the alloy. The application of higher normalization temperature is expected to produce finer and denser MX precipitates after tempering. Additionally, higher normalization temperature tends to increase prior austenitic grain size, i.e., reduce prior austenitic grain boundaries per unit volume, leading to more precipitates at other nucleation sites such as packet boundaries, lath boundaries, and free dislocations. The microstructural evolution induced by the higher normalization temperature tends to improve the performance of base metal as well as weldments [4].

Figure 1. Photo of the as-received Grade 92 plates (heat #011442) procured from CarTech.

Table 3. Procured heats of customized Grade 92.

Heat	Melting	Processing [1]	Product	Plate IDs
011442	VIM+ESR	HF from 1130°C + 1130°C/0.5h/WQ + 600°C/1h/AC + 750°C/1.8h/AC	134-lb. 2"-thick plates	#42X-1, #42X-2
011448	VIM		139-lb. 1.6"-thick plates	#48X-1, #48X-2

Notes: [1] Hot-forging (HF), water quench (WQ), air cooling (AC).

The chemistry of the heats as compared to the ASTM A182-12a is listed in Table 4. The VIM heat (#011448) exhibited a good chemistry control within the ASTM specification. The chemistry variations at the heat locations such as top, center and bottom are negligible. In contrast, the ESR heat (#011442) showed noticeable offset of Nb, N, and B beyond the ASTM specification, which are highlighted in the Table. ESR is a common step used in steelmaking industry to remove impurities and improve homogeneity of ingots. The reasons for the out of control of the three elements as well as Si have been identified, which are resolvable during industrial scale heat production [5].

Table 4. Compositions (wt.%) of the customized Grade 92 heats with Fe as balance of F92 (UNS K92460) with Fe as balance (ASTM A182/A182M-12a).

Heat	Condition	C	Mn	P *	S *	Si	Cr	Mo	Ni	V	Nb	N	W	B *
ASTM A182-12a	Min	.07	.30	-	-	-	8.5	.30	-	.15	.04	.030	1.5	10
	Max	.13	.60	200	100	.50	9.5	.60	.40	.25	.09	.070	2.0	60
011442	Top	.088	.35	<50	9	<.01	8.75	.36	.11	.16	.03	.029	1.79	8
	Center	.088	.35	<50	12	<.01	8.71	.36	.11	.17	.02	.031	1.79	9
	Bottom	.089	.33	<50	6	.02	8.68	.36	.12	.16	.03	.031	1.79	14
011448	Top	.090	.40	<50	6	.09	8.79	.35	.11	.18	.08	.051	1.79	52
	Center	.094	.39	<50	8	.09	8.77	.35	.11	.18	.07	.048	1.79	48
	Bottom	.093	.40	<50	5	.09	8.78	.35	.11	.18	.08	.045	1.78	53

Note: * in ppm; Al, Ti, Zr, Cu < 0.01%; Highlighted wt.% is outside of ASTM A182-12a.

Metallographic microstructure characterization was conducted on samples extracted from plate #48X-1 (VIM heat). The samples were mechanically polished using standard metallography techniques and etched using a solution of $50H_2O/5HNO_3/1HF$. Their optical images are shown in Figure 2 with sampling locations and orientations schematically shown in the inset. Tempered martensite developed in all the samples at different locations, suggesting good microstructural homogeneity. The prior-austenite grain size is about 30-50 μm, comparable to conventional Grade 92, which indicates that the increased normalization temperature did not remarkably increase the prior-austenite grain size.

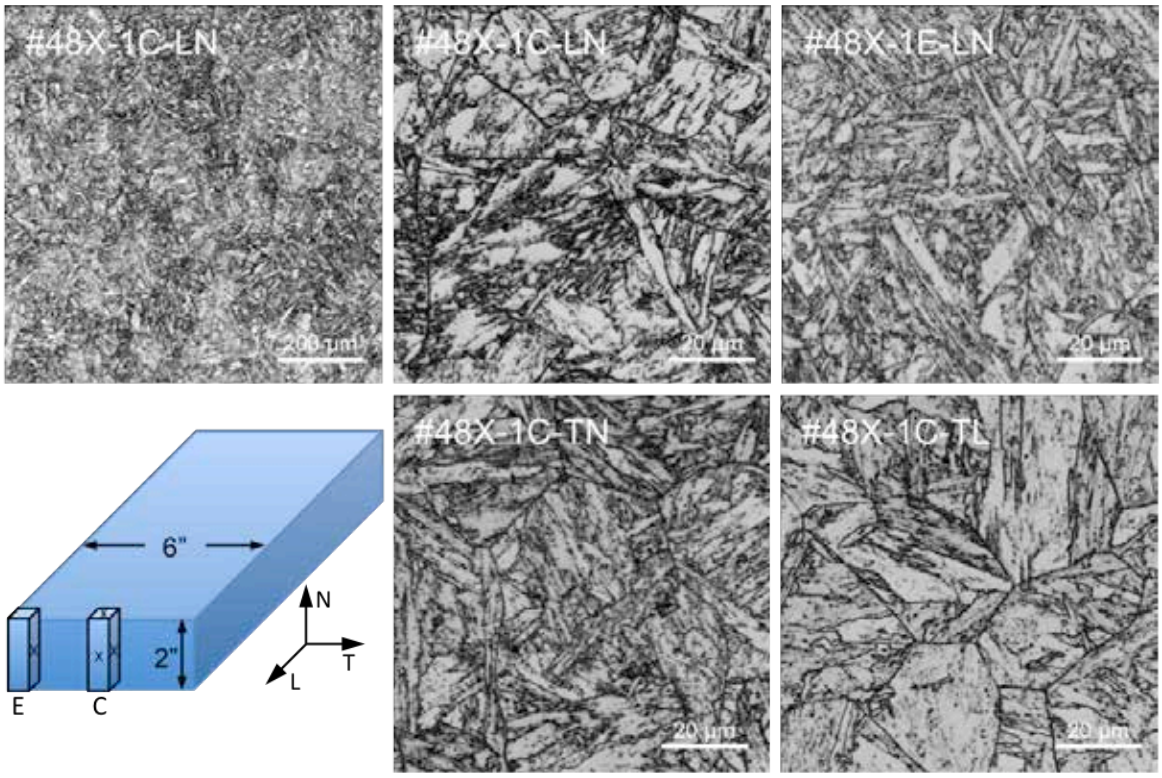

Figure 2. Optical micrographs, taken from different orientations as denoted in the inset, of the as-received Grade 92 heat (Plate #48X-1).

Vickers hardness measurements were conducted on the metallographic samples according to the ASTM standard E384 – 11, "Standard test method for Knoop and Vickers hardness of materials". Three measurements with a load of 1 kgf were conducted for each sample location and orientation. The hardness ranges from 295.3 to 317.5 HV1 with an average of 308.4 ± 6.2 HV1. The measured hardness values do not show significant dependence on the orientations of the samples, suggesting good homogeneity. As compared to the mechanical property requirement of forged Grade 92 (F92) specified in the ASTM A182-12a (Table 5), the measured hardness is greater than the required maximum hardness of 284 HV.

Table 5. Tensile (minimum) and hardness (maximum) requirements of F92 at room temperature.

Tensile strength MPa [ksi]	Yield strength Mpa [ksi]	Elongation in 50 mm [2 in.], %	Reduction of Area %	Hardness Number HBW [HV]
> 620 [> 90]	> 440 [64]	> 20	> 45	< 269 [< 284]

Standard round bar specimens with a ¼" diameter gauge section, as specified in Figure 3, were prepared for tensile testing at room temperature. The length direction of the specimens is parallel to the longitudinal direction of the plates. The specimens were extracted from 1/4-thickness locations of plate #48X-1. Tensile testing was conducted in air at room temperature in accordance with the ASTM standard E8/E8M-13a, "Standard test methods for tension testing of metallic materials." The testing was performed using an MTS tensile testing system with a crosshead speed of 7.9×10^{-3} mm/s (0.0187 in./min). The tensile testing system and load cell were regularly calibrated.

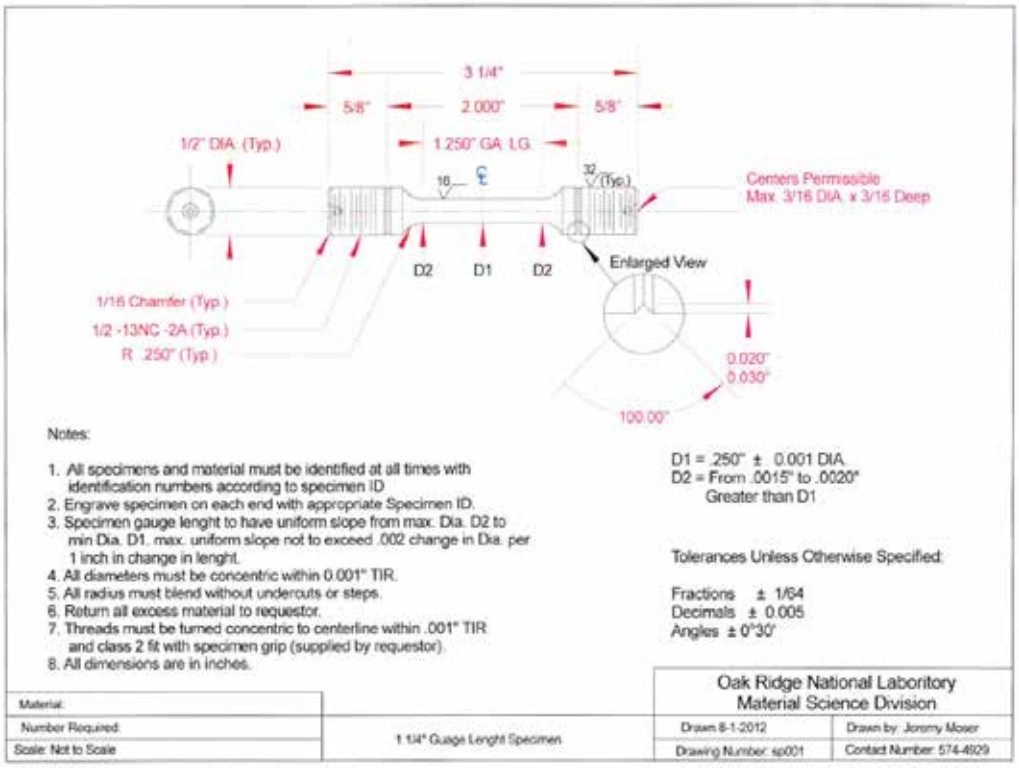

Figure 3. Specification of round bar specimens with a ¼" diameter gauge section.

The tensile curve of the specimen from plate #48X-1 is shown in Figure 4 with yield and tensile strength of 756 and 852 MPa, respectively, and a total elongation of 18.75%. As compared to the requirements listed in Table 5, the procured Grade 92 has superior strength but inferior ductility.

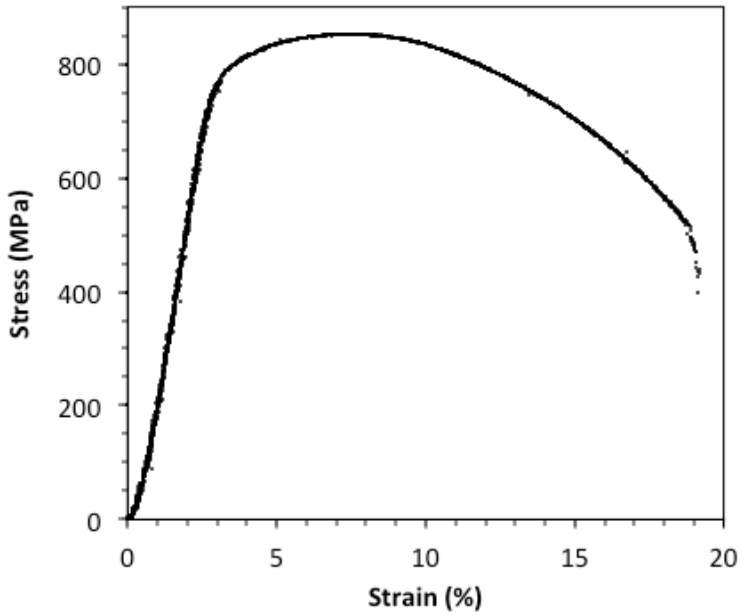

Figure 4. Stress-strain curve of the as-received Grade 92 heat (Plate #48X-1).

Charpy impact resistance is an important property of FM steels, which influences the application condition of the materials. Although Charpy impact resistance is not specified in the ASTM A182-12a, it was conducted on a Tinius Olsen Charpy 300 ft-lb machine according to the ASTM standard E23-12c, "Standard test methods for notched bar impact testing of metallic materials." The measurement calibration of the Charpy machine is performed annually through testing of specimens with certified values to verify the accuracy of the machine. The certified specimens are obtained from the National Institute of Standards and Technology (NIST). Full-size Charpy specimens with a specification shown in Figure 5 were used to screen the absorbed impact energies at room temperature. The specimens were machined from the T-L (transverse-longitudinal) orientation referring to plate #48X-1, which has the worst energy absorption as compared to the other orientations.

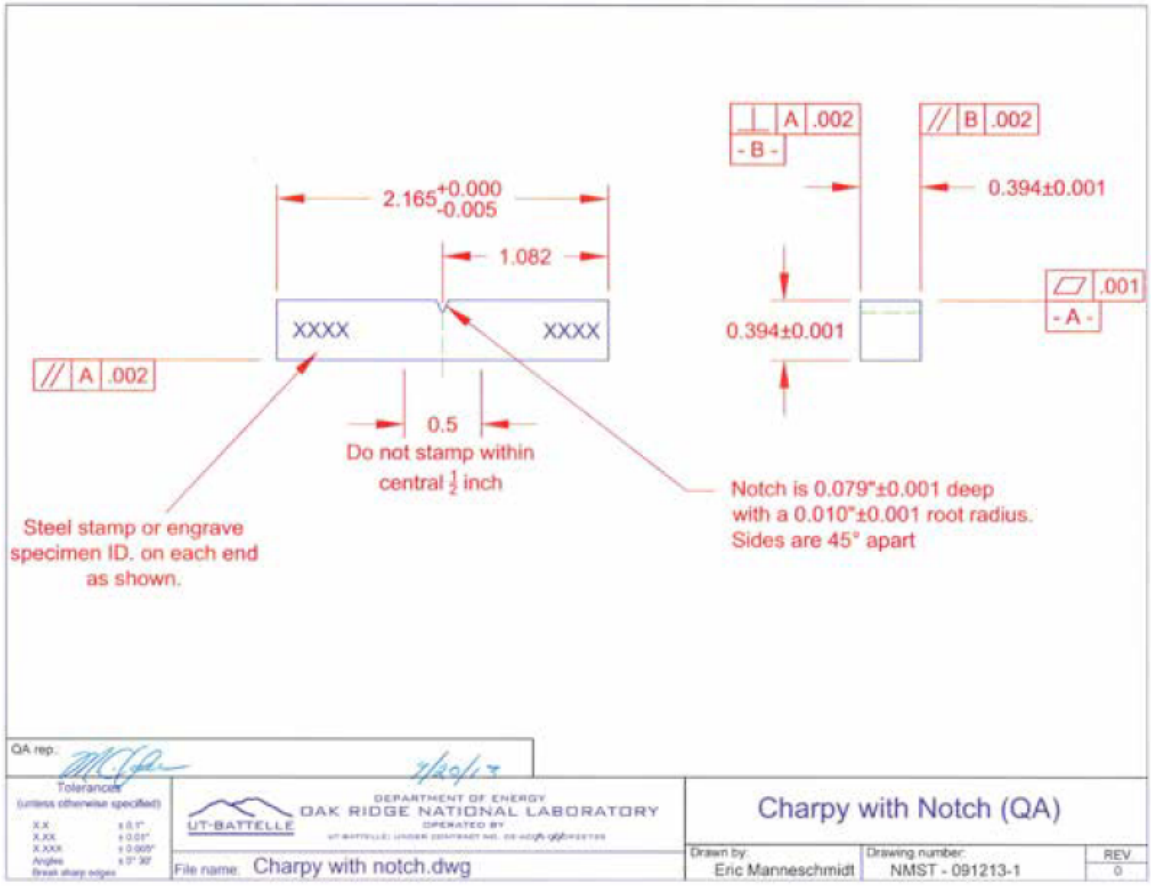

Figure 5. Specification of full-size Charpy specimen.

The specimen in the as-received condition (110 min. tempering at 750°C) yielded a low absorbed energy at the testing temperature of 25°C. This result, together with the hardness and tensile results, suggests that the tempering to the alloy was not enough. Therefore, additional tempering at the same temperature was conducted to the specimens that were individually sealed in a quartz tube under vacuum. The absorbed energies at 25°C of the additionally tempered specimens are plotted in Figure 6. The Vickers hardness of the corresponding specimen conditions were also measured and plotted in Figure 6 for comparison. The absorbed energies at 25°C tended to saturate at ~ 216 J after an additional tempering of 130 min. (or a total of 4 hr tempering). However, hardness continuously decreases with tempering time. A significant reduction in hardness occurred after tempering beyond a total of 4 hr, suggesting an over-

tempering condition. According to the screening results, the plates of #48X-1 and #48X-2 have been tempered at 750°C for additional 130 min, i.e., a total of 4 hr tempering at 750°C for heat #011448. Similar examination will be conducted on heat #011442 (VIM+ESR heat).

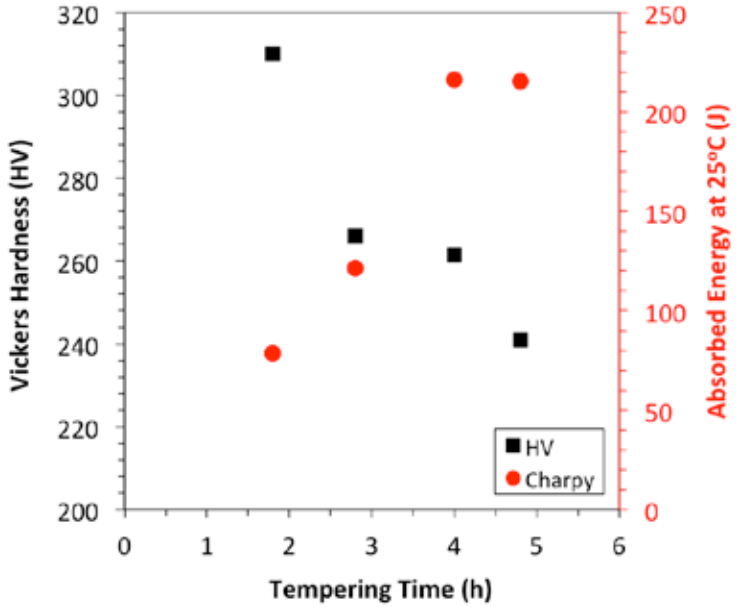

Figure 6. Effect of tempering time at 750°C on the Vickers hardness and Charpy impact absorbed energy at room temperature of the procured Grade 92 heat (Plate #48X-1).

2.2 Alloy 439 (High-Cr Ferritic)

Alloy 439 (UNS S43035) is a high-Cr, ferritic stainless steel, having excellent resistance to stress corrosion cracking (SCC) and intergranular (IG) corrosion. According to the forms of the material, alloy 439 is specified in different designations of the ASTM and ASME standards. Table 6 lists the applicable ASTM and ASME standards of alloy 439. Alloy 439 is also included in the ASME Boiler & Pressure Vessel Code Section I, IV, and VIII Division I and XII.

Table 6. ASTM and ASME designations of alloy 439.

Material Form	Standards
Plate/Sheet/Strip	ASTM A240, ASME SA240
Pipe/Tubing	ASTM A268, ASME SA268, ASTM A803
Bar	ASTM A479, ASME SA479

Alloy 439 in a plate form, preferable for the planned testing in the ARRM program, has been procured from CarTech. The as-received plates of alloy 439 are shown in Figure 7. The heat compositions, listed in Table 7, indicate chemistry homogeneity of the heat, which are within the composition range of alloy 439 specified in the ASTM A240-13a. The contents of Si and Ni were limited to reduce the formation tendency of Ni_3Si-type phase during irradiation of the alloy.

Figure 7. Photo of the as-received plates of Alloy 439 (heat #011438) procured from CarTech.

Table 7. Chemical requirement (wt.%) of alloy 439 with Fe as balance.

Heat	Condition	C	Mn	P	S	Si	Cr	Ni	N	Ti	Al
ASTM	Min.						17.0			0.20+4(C+N)	
A240-13a	Max.	0.030	1.00	0.040	0.030	1.00	19.0	0.50	0.03	1.10	0.15
	VIM-top	0.017	0.4	<0.005	0.001	0.09	17.56	0.20	0.002	0.40	<0.01
011438	VIM-center	0.021	0.4	<0.005	0.001	0.09	17.51	0.21	0.002	0.39	0.01
	VIM-bottom	0.019	0.4	<0.005	0.001	0.09	17.59	0.21	0.002	0.39	<0.01

The VIM ingot was converted into 2”-thick plates by hot forging at 1093°C after soaking the ingot at 1250°C for 2 h. The hot forged plates were air cooled and finally annealed at 850°C for 2 h followed by water quenching to room temperature. Metallographic specimens were extracted from the center and edge of plate (#5) width as schematically shown in the inset of Figure 8. The specimens were polished and etched using a Glyceregia solution being composed of 30 ml glycerol, 30 ml HCl and 10 ml HNO_3. There is no significant difference between the center and edge of the plate width. The grains on the normal-longitudinal (NL) orientation are noticeably elongated along the longitudinal direction of the plate. In contrast, the grains on the normal-transverse (NT) orientation are approximately equiaxed. The grains at the surface are about 200 μm, which increased to about 1-2 mm at plate center. Such larger grain size variations and large grains may suggest that the plates were not processed in a right condition. However, the cross-thickness grain size variation of an alloy 439 in a sheet form (1 mm thick), as shown in Figure 9 [6], also exhibited large grain size variation from about 100 μm at surface to about 1 mm at center.

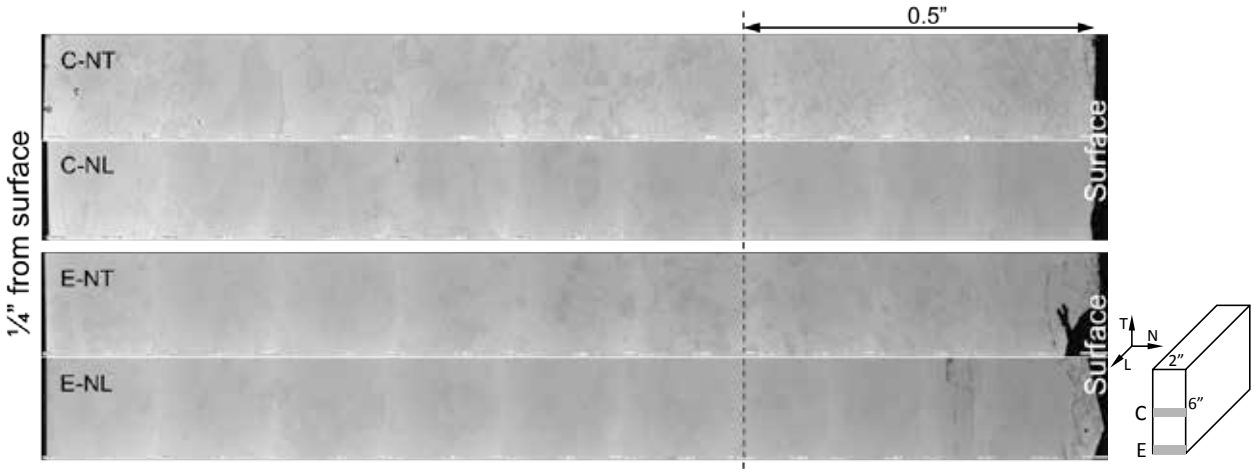

Figure 8. Optical micrographs of the as-procured alloy 439 heat samples extracted from the shaded regions shown in the inset.

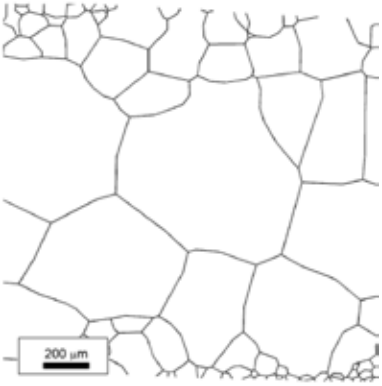

Figure 9. Through thickness grain size variation of an alloy 439 sheet (1 mm thick) [6].

The large grain size variations and large grains are not good for property assessment that are specified in the ARRM program, e.g., ion irradiation, mechanical properties, corrosion resistance, etc. Therefore, thermomechanical treatment (TMT) has been practiced to recrystallize the material with refined and uniform grains across plate thickness. Small sections (3"×3"x2") of the alloy 439 plates were warm-rolled to 0.8" thick at 750, 650, and 500°C, respectively, followed by final annealing at 950°C for 10 min. The cross-thickness optical micrographs are shown in Figure 10. Insignificant amounts of recrystallization occurred in the sample warm rolled at 750°C. Lower warm-rolling temperatures triggered more recrystallization, e.g., the 500°C sample. The high magnification micrograph indicates that some fine precipitates formed during the 500°C TMT in addition to the large primary Ti(C,N) in a few micrometers. Although the 500°C TMT exhibited good grain refinement with an average size of ~100 µm, some grains are not fully recrystallized, e.g., the up-right corner of the 500°C micrograph at a low magnification in Figure 10. These partially recrystallized grains retain the deformed shape along the rolling direction.

Vickers hardness of the alloy 439 samples in the as-received and the TMT conditions was measured using a load of 1 kgf. As compared to the as-received condition having a hardness of 136.0 ± 6.4 HV1, the hardness of the 750°C warm-rolled sample was slightly increased to 139.4 ± 3.2 HV1. In contrast, the hardness of the samples warm-rolled at 650°C was decreased to 134.8 ± 11.0 HV1 and at 500°C to 128.2 ± 3.0 HV1. The hardness changes are consistent with the occurrence of recrystallization that softens the

alloy. The hardness results satisfy the requirement of alloy 439 specified in the ASTM A240-13a as listed in Table 8.

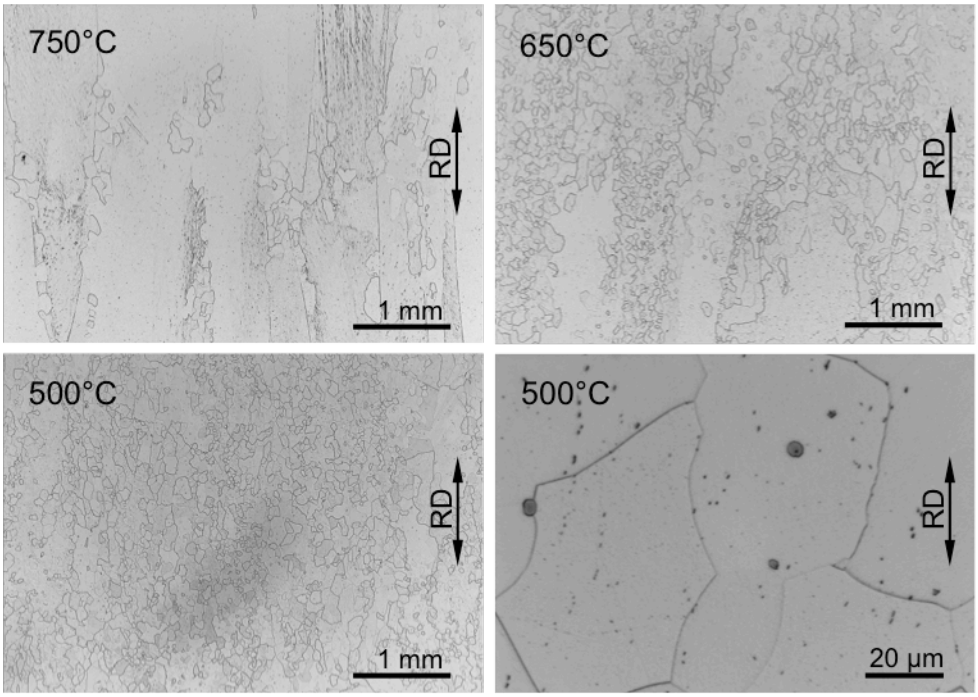

Figure 10. Optical micrographs of the warm-rolled samples at 750, 650, and 500°C followed by annealing at 950°C for 10 min.

Table 8. Tensile, hardness, and bending test requirements of alloy 439 (UNS S43035).

	Yield MPa	Tensile MPa	Elongation in 50 mm [2 in.], %	Hardness HRB (HV)	Cold Bend* Degree	Charpy
ASTM A240-13a	>205	>415	>22	<89 (<180)	180	Lateral expansion opposite the notch ≥ 0.38 mm (0.015 in.)

* Cold bend test is not required for plate thicker than 25 mm [1 in.]

The TMT results indicate that TMT at lower temperatures is needed to obtain completely recrystallized microstructure for the prescribed amount of deformation. Further TMT studies will be pursued on alloy 439 to obtain a well-controlled grain size distribution. Tensile, bending, and Charpy impact tests will be conducted on the processed alloy 439 to verify their properties according to the ASTM A240-13a as listed in Table 8.

2.3 14YWT (9-14Cr ODS)

ODS alloy 14YWT with potential both low and high strength applications is selected for testing in the ARRM program. The alloy, also named as nanostructured ferritic alloy (NFA), was developed under the DOE Fuel Cycle Research & Development (FCRD) program. The advanced ODS FCRD-NFA1 heat was produced using a new approach for preparing Ar gas atomized powders that consisted of directly adding yttrium (Y) to the melt prior to gas atomization and controlling the O level in the powders. Research and

development on ball milling experiments at ORNL using the Simoloyer CM08 have been improved to reduce the contamination levels of primarily C and N in the powders during ball milling. These conditions were provided to Zoz, GmbH, Germany, for ball milling the powders produced with the new approach. The following describes the steps in the production of the FCRD-NFA1 plates for the ARRM program, which used the "best practice" processing condition developed in the FCRD Advanced Fast Reactor Cladding Program.

2.3.1 Production and Ball Milling of Pre-Alloyed Powder

The advanced ODS FCRD-NFA1 ferritic alloy was produced by mechanical alloying (MA) using a new approach for preparing Ar gas atomized powders that consisted of directly adding yttrium (Y) to the melt prior to gas atomization and controlling the O level in the powders. It is generally recognized that ball milling can result in high contamination levels, especially for interstitial O, C and N atoms, in powders. Such high contamination levels are undesirable. For this reason, the research conducted in the FCRD Advanced Fast Reactor Cladding Program has focused on minimizing the C and N levels and controlling the O level during ball milling. Recent ball milling experiments using the high kinetic energy CM08 Simoloyer at ORNL have been successful in reducing the O, C and N levels in powders.

Pre-alloyed powder with composition Fe - 13.8Cr - 3.0W - 0.37Ti - 0.21Y - 0.012O (wt. %) was prepared by Ar gas atomization by ATI Powder Metals. A total of ~55 kg of powder was produced and sieved into three lots of -35/+100 mesh (150-500 μm), -100/+325 mesh (45-150 μm) and -325 mesh (<45 μm). Chemical analysis of the atomized powder indicated that the specified compositions for the alloying elements, including the addition of Y to the melt, and interstitial O, C and N levels were achieved by ATI Powder Metals.

The three sieved lots of pre-alloyed powders were shipped to Zoz for ball milling at the pilot facility in Wenden, Germany. Powder from the V540-02 lot was used for producing the FCRD-NFA1 heat. The V540-02 lot consisted of blended powders of -100/+325 mesh and -325 mesh sizes. The powder was ball milled for 40 h in Ar gas using the high kinetic energy CM100 Simoloyer. The ball milling parameters were supplied by the FCRD processing team to Zoz for the ball milling runs. The results of the chemical analysis shown in Table 9 revealed that the ball milling conditions resulted in low C and N levels, with O near the targeted concentration level in the powder.

Table 9. Chemical analysis results of ball milled powder (V540-02).

Fe	Cr	W	Ti	Y	O	C	N
Bal.	12.77	2.95	0.38	0.22	0.125	0.014	0.007

2.3.2 Extrusion and Fabrication of FCRD-NFA1 Plates

Ball milled powder of the V540-02 lot was supplied by the FCRD program for producing two extrusions of the FCRD-NFA1 ferritic alloy. Two cans were fabricated from 304L stainless steel stock with dimensions of 9.9 cm diameter and 21.6 cm in length. Each can was filled with ~2.25 kg of ball milled powder, degassed at 400ºC and then sealed. The cans were heated at 850ºC for 2 hr and extruded through a 6.35 cm × 3.05 cm in a rectangular die to produce extruded bars of the FCRD-NFA1. An example of an extruded bar is shown in Figure 11. The leading and trailing ends of each extruded bar was cut off to produce ODS sections that were ~37.5 cm long. Each bar was cut into ~3 equal lengths and annealed at 1000ºC for 1 hr in high vacuum. The 6 bar sections were rolled into plates normal to the

extrusion direction at 1000ºC to 50% reduction in thickness (RIT). Figure 12 shows the ODS FCRD-NFA1 plates enclosed in the 304L SS can (left) and after being machined off, i.e. decanning (right).

Figure 11. Photo of the extruded FCRD-NFA1 bar.

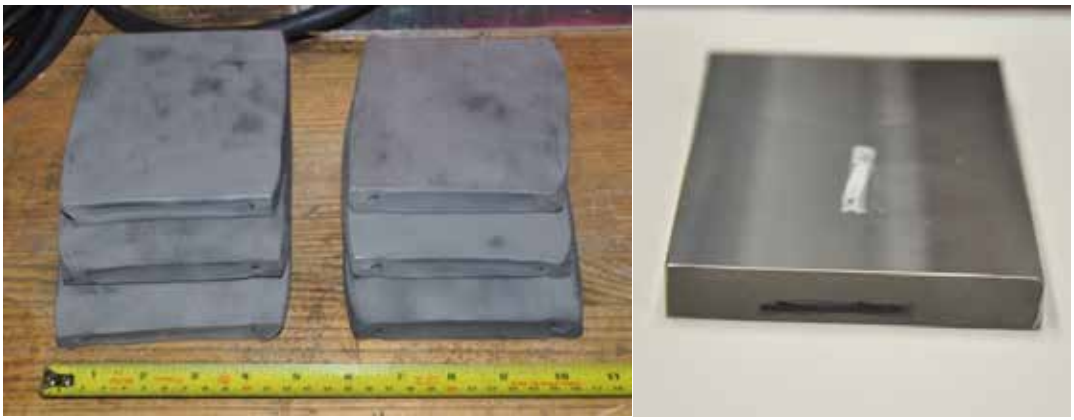

Figure 12. Photo of the six fabricated FCRD-NFA1 plates with the 304L stainless steel can intact (left) and one plate after decanning (right).

2.3.3 Microstructure and Hardness Characterizations

Scanning electron microscopy (SEM) employing secondary (SE) and backscattered (BSE) electron imaging was used for characterizing the microstructure of specimens prepared from the plate. Specimens were cut from the plate in two orientations and prepared by metallographic procedures. With reference to Figure 13, one specimen was cut and mounted with the surface containing the LT orientation, where L is parallel to the extrusion direction and T is parallel to the rolling direction. This orientation showed the top surface of the plate and revealed the effect of cross rolling on the grain morphology. The second specimen was cut and mounted with the surface containing the LN orientation, where L is parallel to the extrusion direction and N is parallel to the thickness direction of the plate. The LN orientation showed the effect of rolling to 50% RIT on the grain morphology in the microstructure. After grinding and polishing with successively finer media, a final polishing step using colloidal silica was used in preparation of the specimens. No etchant was used after polishing. The polished specimens were examined on a JEOL 6500FEG (Field Emission Gun) SEM.

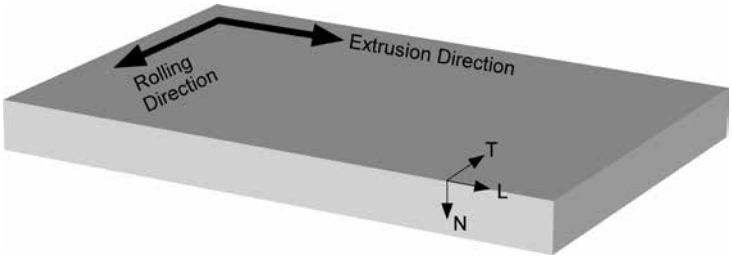

Figure 13. Schematic showing the extrusion and rolling directions fro the FCRD-NFA1 plate and the L-T-N orientation used for preparing the metallographic specimens.

The microstructure observed for the specimen in the LT orientation is shown in Figure 14-16. At low (500X) magnification, a small volume fraction of porosity was observed using SE (Figure 14a) and an apparent bimodal grain size distribution was observed using BSE (Figure 14b). The BSE image shows contrast variations for grains in the microstructure due to electron channeling effects that are sensitive to grain orientation [7]. At higher magnification, the grain morphology became more apparent and stringers of small particles were visible in the microstructure as shown in Figure 15. The grains appeared nearly equiaxed since no significant elongation in either the extrusion (horizontal axis) or rolling (vertical axis) were observed. The particles associated with stringers were ~20-150 nm in size and appeared with dark contrast in BSE images, indicating that their crystal structure consists of low-Z (atomic number) elements. At the lower (2kX) magnification (Figure 15a), the stringers showed wavy patterns and were not aligned preferentially with either the extrusion or rolling directions. In addition, the particles do not appear to have formed with any preference to grain boundaries as observed at higher (5kX) magnification (Figure 15b). Another characteristic of many larger grains that were observed at low magnifications was that subtle contrast differences were observed in BSE images at higher magnifications. The BSE image shown in Figure 16 was obtained at a higher (10kX) magnification (inset observed in Figure 15b) to illustrate this. The arrows point to larger grains that showed contrast variations within. These observations are consistent with low misorientations between several grains in regions of the microstructure due to texture that collectively can give the appearance of a larger grain at low magnifications.

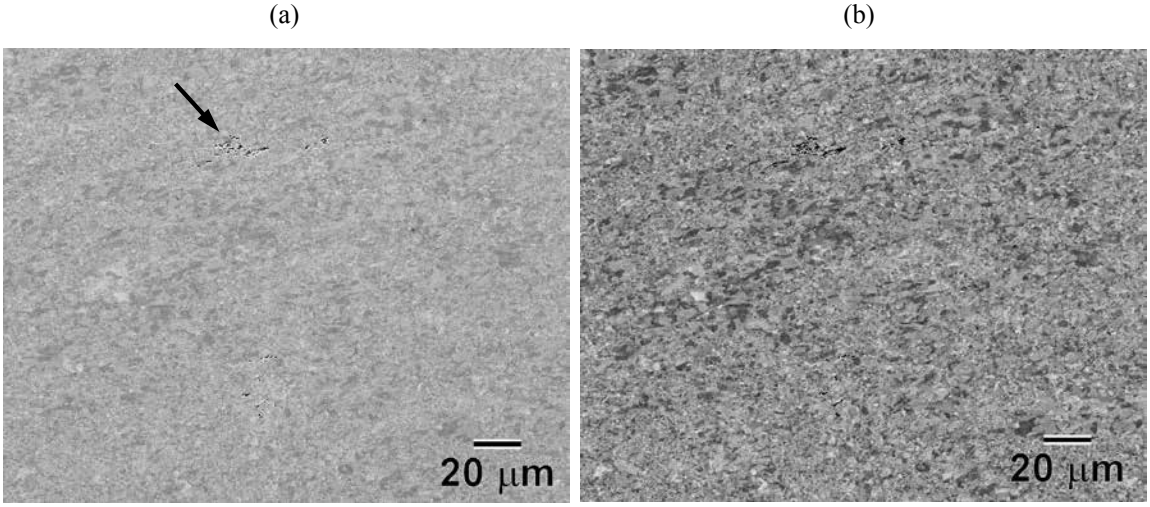

Figure 14. LT orientation: (a) SE image showing porosity and (b) BSE image showing apparent bimodal grain size distribution.

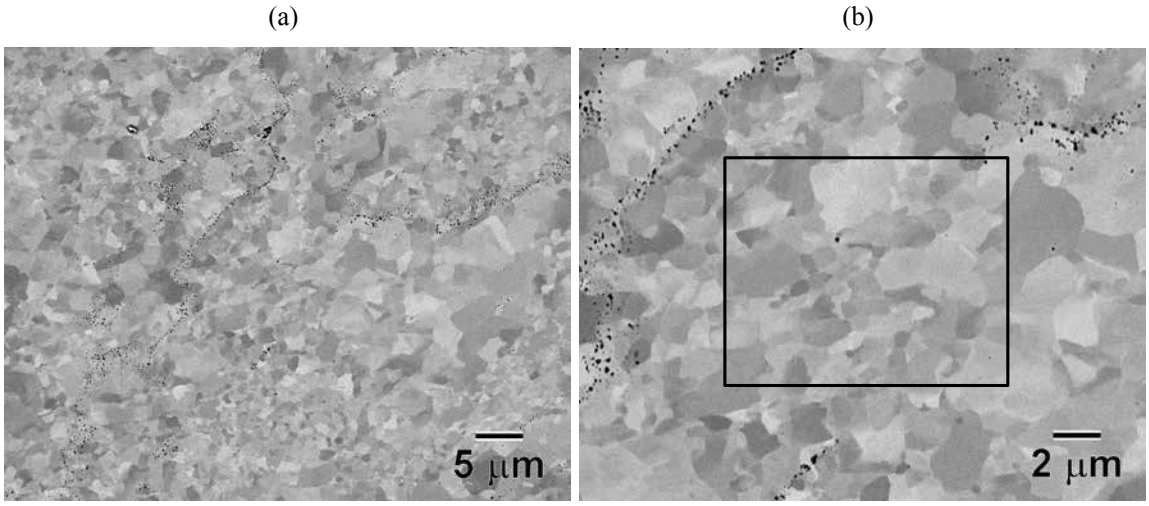

Figure 15. LT orientation BSE images showing stringers of small particles in dark contrast at (a) low (2 kX) magnification and (b) higher (5 kX) magnification. The inset in Figure 15b defines the area viewed at a higher magnification in Figure 16.

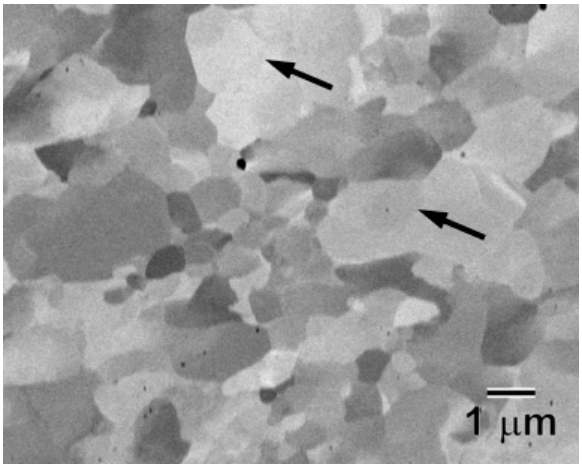

Figure 16. LT orientation BSE image of inset in Figure 15b at a higher (10 kX) magnification showing contrast variations in grains which are not apparent at lower magnifications.

The microstructure observed for the specimen in the LN orientation is shown in Figure 17-19. At low (1kX) magnification, several regions of porosity were observed using SE (Figure 17a) and the grain morphology appeared distorted in the extrusion direction (horizontal axis) using BSE (Figure 17b). In some locations of the microstructure, a packet of large grains was observed as shown in Figure 18. The grains associated with this packet were elongated in the extrusion axis and most likely were associated with a single ball milled particle. At high magnifications, the elongated grain morphology and stringers of small particles became apparent as shown in Figure 19. The grains were elongated in the extrusion direction, with some showing extensive elongations. Plus, in Figure 19b, the stringers of particles showing dark contrast were also preferentially aligned in the extrusion direction.

(a) (b)

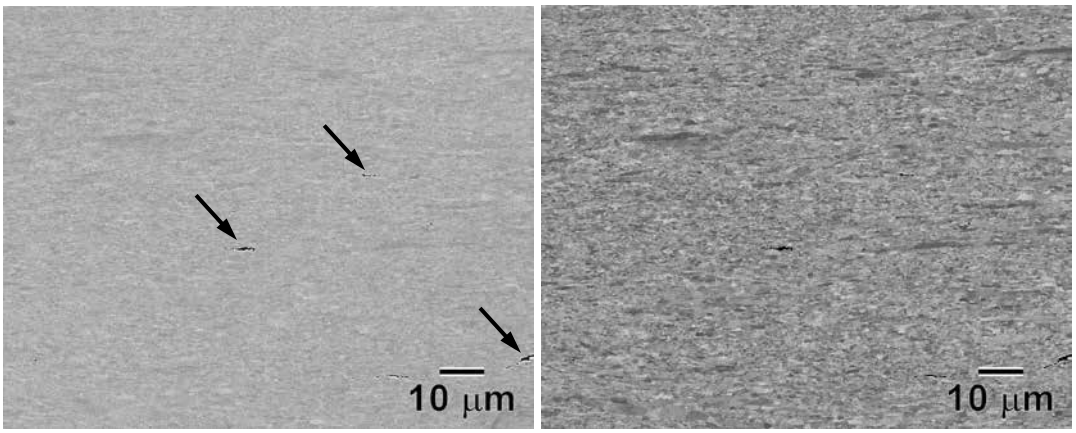

Figure 17. LN orientation: (a) SE image showing porosity and (b) BSE image showing apparent bimodal grain size distribution.

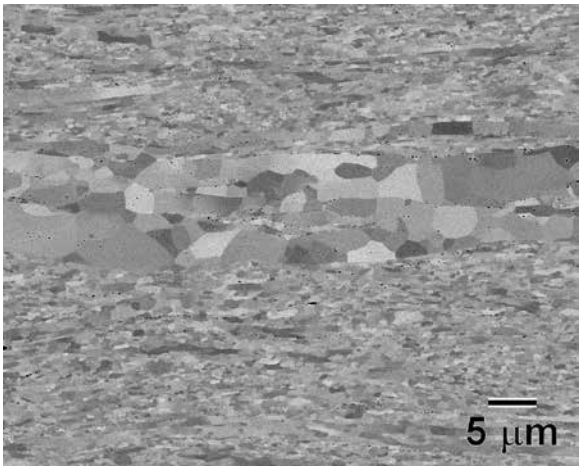

Figure 18. LN orientation BSE image showing a packet of large grains elongated in the extrusion direction.

(a) (b)

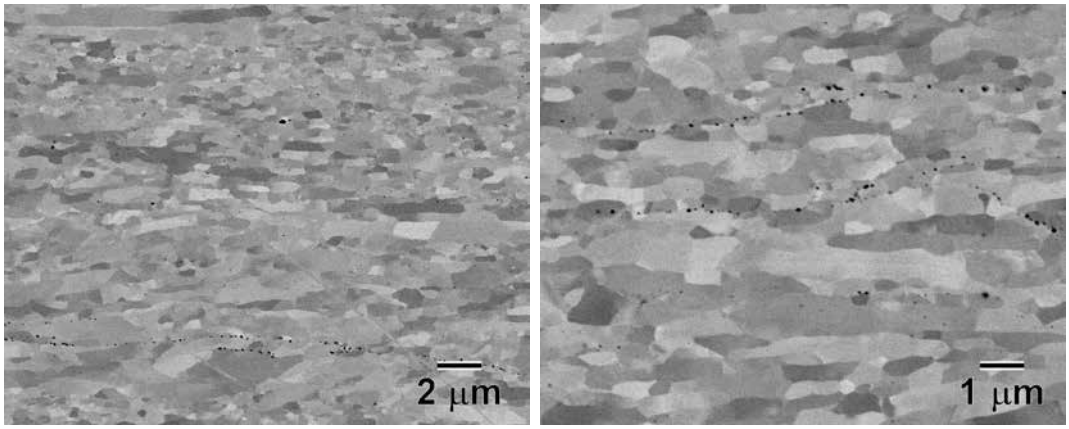

Figure 19. LN orientation BSE images showing (a) elongated morphology of the grains and (b) stringers of particles with dark contrast.

Grain size measurements were conducted on the specimens in the LT and LN orientations. The average grain size (*D*) was obtained by the line intercept method in terms of the 95% confidence interval in the standard error of the mean [8]. The grain size was measured parallel to the extrusion and to the rolling (LT) or thickness (LN) directions to determine the grain aspect ratio (GAR). The results of the grain size measurements for both orientations are shown in Table 10. For the LT orientation, the values of the grain size measured in the extrusion and rolling directions were similar in both the average and the standard error, which was the reason for the low GAR value of 1.02. This result indicated that rolling normal to the extrusion axis to 50% RIT was effective in minimizing the anisotropy in grain morphology caused by extrusion. For the LN orientation, the grain size measured in the extrusion direction (0.789 ± 0.54 μm) was close to that measured in the same direction in the LT orientation (0.779 ± 0.047 μm). However, the grain size measured in the thickness direction was much smaller (0.473 ± 0.023 μm), which accounted for the larger GAR of 1.69. This result indicated that rolling to 50% RIT caused more significant distortion in the grain morphology in the thickness direction than in the extrusion direction. Since the volume of the grains should be conserved during plastic deformation, it would be expected that the grains are similarly distorted in the rolling direction, which could be observed if a specimen had been prepared in the TN orientation.

Table 10. Measurements of grain size and grain aspect ratio (GAR) in the LT and LN orientations.

Orientation	Grain Size (mm)		GAR
	Parallel to Extrusion Axis	Parallel to Rolling Axis	(PEA/PRA)
LT	0.779 ± 0.047	0.764 ± 0.044	1.02
LN	0.789 ± 0.054	0.473 ± 0.023	1.69

Note: 95% confidence interval = $\bar{x} \pm 2$ S.E., where $\bar{x}$ is the mean and S.E. is standard error of the mean.

Vickers hardness measurements were obtained on polished surfaces of the specimens in the LT and LN orientations. The procedure consisted of obtaining 7 random measurements for the LT orientation and 7 measurements spanning the thickness of the LN orientation, starting near the top surface and ending near the bottom surface. The measurements were obtained using a 200 g load. The results showed that the average hardness value for the LT orientation was 364.3 ± 13.9 HV0.2 and for the LN orientation was 369.0 ± 9.4 HV0.2. These values agreed quite reasonably for both orientations. In addition, Figure 10 shows the hardness values obtained from the thickness measurements in the LN orientation. The results indicated that the 50% RIT during rolling did not introduce any significant non-uniformity in the microstructure of the plates, at least at the macroscopic level.

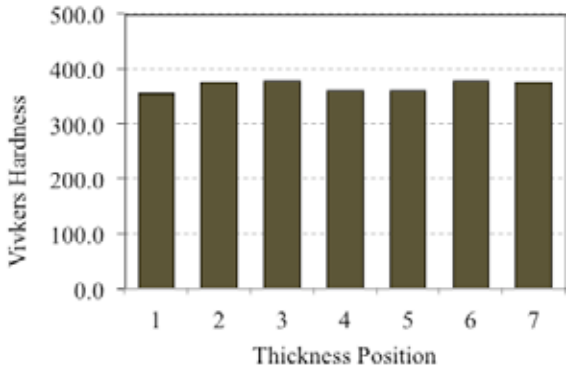

Figure 20. Vickers hardness values obtained as a function of thickness position in the plate in the LN orientation.

2.3.4 Discussion

Compared to the grain size of many previously produced heats of 14YWT during the past 12 years, the grain size measured for FCRD-NFA1 was larger. For example, the SM10 heat of 14YWT produced in 2007 contained a grain size of ~160 nm, or 0.160 μm [9]. However, the SM10 heat also contained a much higher concentration of O, C and N, due to contamination of the powder during ball milling, compared to the FCRD-NFA1, as well as more recent heats of 14YWT such as SM12 [10]. But like FCRD-NFA1, the grain size of SM12 was comparable in size, i.e. 0.732 +/- 0.073 μm for the heat that was extruded at 850ºC [11]. Thus, the "cleaner" variants of 14YWT including the FCRD-NFA1 are characterized as having larger grain sizes. The reason for this observation is not clearly understood, but detailed microstructure analysis of the 14YWT-SM12 heat revealed the typical high number density of Ti-, Y- and O-enriched nanoclusters within grains and along grain boundaries [11]. Thus, the increase in grain size for the "cleaner" ODS variants of 14YWT cannot be accounted for by differences in the dispersion of nanoclusters, but must be due to other factors associated with high interstitial O, C and N levels.

Although particles showing dark contrast in BSE images have been observed in previous 14YWT heats, the distribution of these particles as wavy stringers appears to be associated with the FCRD-NFA1 heat. Backscattered electrons are produced from elastic scattering of the primary beam that scales with the backscattered electron coefficient, η, which increases with Z [7]. Therefore, the dark contrast associated with the particles most likely means that they do not contain Y or W elements, but is consistent with Ti-rich particles. Several types of Ti-rich phases have been identified in 14YWT heats, such as Ti-rich oxide, TiO_2 and Ti(O,C,N) particles that are typically larger than ~20 nm [12,13,14]. Furthermore, recent LEAP analysis of FCRD-NFA1 identified particles larger than ~20 nm as Ti(C,N) [15]. The results for FCRD-NFA1 showed that these particles formed in wavy patterns that were not aligned with either the extrusion or rolling directions in the LT orientation (Figure 15) and were not preferentially located on grain boundaries. These observations suggest that their formation during the 850ºC anneal prior to extrusion must have been affected by local concentration variations of Y and Ti in the ball milled powder. It is surmised that if the Y content was lower in regions of the ball milled particles, this would then lead to enhanced formation of Ti-rich particles instead of Ti-, Y-, O-enriched nanoclusters. This possibility will need to be confirmed with TEM analysis, which will be conducted in the future. However, as mentioned in the experimental procedure, the powder used to produce the FCRD-NFA1 plates was Ar gas atomized with the inclusion of 0.2%Y, which was a challenging task. Unpublished results obtained from electron microprobe analysis (EPMA) of Ar gas atomize particles during development of FCRD-NFA1 in the FCRD Program showed statistical variations in both the Y content per particles as well as within each particle, whereas the Ti content was much more evenly distributed in each particle analyzed. Ball milling for 40 h improved the distribution of Y considerably in the particles analyzed by EPMA, but this was determined at the macroscopic instead of microscopic scale. It may be possible that the non-uniform distribution of Y (as an Fe-Y intermetallic phase on grain boundaries and triple point junctions) in the Ar gas atomized powders may present a greater challenge for ball milling to distribute evenly in the powder, compared to the traditional MA approach where Y_2O_3 particles are ball milled with the Fe-alloyed particles. Further research needs to be conducted to determine the reason for the formation of a high concentration of Ti-rich particles with the wavy pattern in FCRD-NFA1. However, lowering the Ti content in the atomized powder may also contribute to lowering the concentration of Ti-rich phases, which implies further alloy development.

The microstructural analysis showed a distinct bimodal grain size in FCRD-NFA1 (Figure 15 and Figure 19). To some extent, texture may play a role with the appearance of larger grains, but there may be other factors to explain this observation as well. As suggested above, one possibility is that Y may not be

uniformly distributed in the ball milled powders at the microscopic scale. In previous 14YWT heats produced by the traditional MA approach, the grains are often more uniform in size and smaller. To account for this, microstructural investigations have shown that a high concentration of nanoclusters and small oxide particles decorate the boundaries, which then act as Zener pinning sites that hinder further grain growth. A unimodal grain size implies that Y is distributed uniformly in the ball milled powder and that this would favor a high heterogeneous nucleation rate for the nanoclusters and oxide particles on grain boundaries during the pre-extrusion annealing. Since the same procedure was used for extruding the FCDR-NFA1 ball milled powder, differences in the heterogeneous nucleation rate of particles on grain boundaries are most likely responsible for formation of the bimodal grain size. Whether this was affected by non-uniformity in the Y distribution will need further detailed microstructural analysis which is planned.

2.4 12Cr FM Steel and High-Cr&Al ODS Alloy

Specific alloys in the alloy groups of 12Cr FM steel and high-Cr&Al ODS alloy have not been determined. Alloy HT-9 was initially selected in the 12Cr FM alloy group due to its availability of comprehensive data compared to other alloys in this group. However, its irradiation embrittlement occurs after neutron irradiation below 400°C may significantly limit its applications in the LWR condition. It's not easy to alleviate the low-temperature irradiation embrittlement in the HT-9 chemistry, which is generally induced by irradiation hardening, radiation-induced precipitation and helium production. Based on the commercialized PM2000 and MA956 and the recently developed 16Cr-4.5Al ODS alloy, new high-Cr&Al ODS alloys are being developed for accident tolerant fuel cladding applications under the DOE Fuel Cycle Research & Development (FCRD) program. It is expected to receive invaluable insights from this study to guide a selection of a candidate alloy in the high-Cr&Al ODS alloy group.

3. PROCUREMENT OF REFERENCE ALLOYS

Stainless steel 316L is selected as a reference steel due to its large amount of available data from the LWR relevant conditions. A 316L stainless steel plate in a size of 81.3 × 81.3 × 2.5 cm^3, as shown in Figure 21, has been procured from Earle M. Jorgensen Company with a composition of Fe-0.0191C-16.5795Cr-0.4895Cu-1.4910Mn-2.0255Mo-0.0456N-10.0350Ni-0.0355P-0.0018S-0.2685Si in weight percentage (wt.%).

Figure 21. Photo of the as-received 316L stainless steel plate (32”×32”×1”).

Additionally, a few pieces of commercial T92 (tube form of NF616) with an amount of ~200 lbs. have been procured from Nippon Steel of Japan to be served as a reference steel of 9Cr FM steels. The T92 heat is in a form of 1-1/4” outer diameter with a 1/4” wall thickness. The microstructures and basic mechanical properties of the as-received 316L and T92 will be assessed.

4. SUMMARY

A total of sixteen down selected commercial and advanced alloys are being procured for testing under the ARRM program. EPRI-GE is leading the procurement of eleven commercial alloys. Most of the commercial alloys (eight out of eleven) have been procured. ORNL is leading the procurement of advanced alloys, including customized Grade 92, customized alloy 439, 14YWT ODS alloy, and two other alloys that are to be determined in the alloy groups of 12Cr FM and high-Cr&Al ODS alloy. The procured commercial and advanced alloys will be stored and organized at EPRI and ORNL, respectively. A material tracking system is being established and used at EPRI and ORNL during the progress of the ARRM program.

The customized Grade 92 and alloy 439, fabricated by means of VIM/ESR and hot forging, have been procured from CarTech. Each alloy has a nominal weight of 400 lbs. and in the form of plates (2"-thick). The 14YWT ODS alloy (~10 lbs.) has been extruded, cross-rolled and decanned at ORNL. Additionally, reference alloys, i.e., 316L and T92 (tube form of NF616) have been procured from two vendors. Table 11 summarizes the procurement status of advanced alloys and reference alloys for the ARRM program.

Table 11. Procurement status of advanced alloys for the ARRM program.

Group	Alloy	Identified Alloy	Producer	Available Time
Advanced	9Cr FM	Customized Grade 92	CarTech	May 2014
	12Cr FM	TBD		
	High-Cr FM (>14Cr)	Customized Alloy 439	CarTech	March 2014
	9-14Cr ODS	14YWT	ORNL	May 2014
	High-Cr&Al ODS	TBD		2015
Reference	316L		North American Stainless	September 2014
	T92		Nippon	May 2014

The procured heats of Grade 92 and alloy 439 have been assessed according to relevant ASTM standards and general materials quality requirement, e.g., chemistry homogeneity, microstructural uniformity, tensile, hardness, and Charpy impact resistance. The as-received Grade 92 showed good chemistry control for the VIM heat (#011448). The additional ESR process resulted in significant reductions in the amounts of Si, Nb, N, and B of the VIM+ESR heat (#011442). Samples of heat #011448 exhibited tempered martensite uniformly developed in the material. The hardness and yield strength of the heat are greater than the requirements specified in the ASTM A182-12a, leading to a low absorbed Charpy impact energy at room temperature. Experiments on additional tempering of the samples indicated that a total of 4 hr tempering at 750°C will provide a balanced properties in terms of Charpy impact resistance and strength. Therefore, this type of additional tempering has been applied to the plates of heat #011448. Similar studies on heat #011442 will be pursued.

The as-received alloy 439 heat (#011438) exhibited chemistry and hardness satisfying the ASTM A240-13a. The grain size across plate thickness ranges from ~200 μm at surfaces to about 1-2 mm at plate center. To obtain refined grain size with much smaller size variations, TMT has been conducted on small pieces of the alloy 439. It has shown that lower temperature warm rolling, e.g., 500°C, developed recrystallized grains in the order of 100 μm in most of the processed material. Further TMT studies will be conducted to obtain completely recrystallized microstructure in alloy 439.

Six plates (approximately 4.75"×2.75"×0.35" each) of 14YWT ODS alloy, recently renamed as FCRD-NFA1, have been produced by extruding ball milled powder at 850ºC and cross-rolling to 50% thickness reduction. The plates were produced using the "best practice" processing conditions developed

in the FCRD Advanced Fast Reactor Cladding Program and the extrusion and rolling conditions developed over the past 12 years at ORNL from producing numerous heats of the advanced 14YWT ODS ferritic alloy. The conditions consisted of an unique Ar gas atomization approach that introduced Y into the pre-alloyed (Fe - 13.8Cr - 3.0W - 0.37Ti - 0.21Y - 0.012O; wt. %) powder melt and improved ball milling conditions, resulting in lower C and N contamination levels and better control in the O level of the powder. Characterization studies of the microstructure and basic mechanical properties of the FCRD-NFA1 were initiated. The grain structure observed by SEM analysis consisted of sub-micron size grains that were equiaxed in the LT orientation with a GAR of ~1 and elongated in the LN orientation with a GAR of ~1.7, due to the effects of cross-rolling (former) and 50% thickness reduction (latter) on the grain morphology. The hardness measurements were consistent by showing no macroscopic variations in the microstructure. However, the results also showed a higher than normal concentration of ~20-150 nm size particles (believed to of the Ti(O,C,N) distributed in wavy patterns in the microstructure (LT orientation) and a modest bimodal grain size distribution. Both of these results may indicate that the Ti content of future alloy development efforts may need to be lowered.

REFERENCES

[1] E.A. Kenik, J.T. Busby, Radiation-induced degradation of stainless steel light water reactor internals, Mater. Sci. Eng. R 73 (2012) 67-83.

[2] F.A. Garner, Radiation damage in austenitic steels, in: R.J.M. Konings, T.R. Allen, R.E. Stoller, S. Yamanaka, Comprehensive Nuclear Materials, Elsevier, The Netherlands, 2012.

[3] Critical Issues Report and Roadmap for the Advanced Radiation-Resistant Materials Program, EPRI, Palo Alto, CA and the U.S. Department of Energy, Washington, DC: 2012. 1026482.

[4] C.R. Das, S.K. Albert, A.K. Bhaduri, G. Srinivansan, B.S. Murty, Effect of prior microstructure on microstructure and mechanical properties of modified 9Cr-1Mo steel weld joints, Mater. Sci. Eng. A 477 (2008) 185-192.

[5] L. Tan, Y. Yamamoto, T.-L. Sham, FY14 materials procurements and related examinations of optimized Grade 92 and Alloy 709 steels, ORNL/TM-2014/258, July 22, 2014.

[6] E.R. Homer, B.L. Adams, R.H. Wagoner, Recovering grain-boundary inclination parameters through oblique double sectioning, Metall. Mater. Trans. A 38 (2007) 1575-1586.

[7] D.E. Newbury, D.C. Joy, P. Echlin, C.E. Fiori and J.I. Goldstein, Advanced Scanning Electron Microscopy and X-ray Microanalysis, Plenum Press, New York, (1986).

[8] R.T. DeHoff, Chapter 7: Problem Solving using Quantitative Stereology, in *Applied Metallography*, Ed: G.F. Vander Voort, Van Nostrand Reinhold Company, New York, (1986), P. 89-99.

[9] J.H. Kim, T.S. Byun, D.T. Hoelzer, S.W. Kim and B.H.Lee, Materials Science & Engineering A, Volume 559, (2013), p. 101-110.

[10] D.T. Hoelzer, K.A. Unocic, E.T. Manneschmidt and M.A. Sokolov, Fusion Reactor Materials Program, DOE/ER-0313/52-Volume 52, (2012), p. 33-46.

[11] D.T. Hoelzer, K.A. Unocic, M.K. Sokolov and T.S. Byun, To be submitted to Journal of Nuclear Materials, (2014).

[12] J. Bentley, D.T. Hoelzer, D.W. Coffey and K.A. Yarborough, Microscopy and Microanalysis, Volume 10, Supplement 2, (2004), p. 662-663.

[13] M.K. Miller, D.T. Hoelzer and K.F. Russell, Materials Science Forum, Volume 654-656, (2010), p. 23-28.

[14] M.K. Miller and C.M. Parish, Materials Science and Technology, Volume 27, Number 4, (2011),, p. 729-734.

[15] N.J. Cunningham, Y. Wu, G.R. Odette, D.T. Hoelzer and S.A. Maloy, Fusion Reactor Materials Program, DOE/ER-0313/54-Volume 54, (2013), p. 15-26.